Chapter 10
Mechanistic Aspects of Fracture II ~ Plasticity-Dominated Fracture Models

10.1 Outline of Elemental Concepts of Ductile Fracture

The contrastive picture to decohesion is the so-called microvoid coalescence (MVC) that designates the process in which fracture proceeds by the successive nucleation, growth and linkage of voids. The surface of MVC fracture is characterized by dimple patterns. However, MVC process can take place in very fine scale with macroscopically irregular or crack-like appearances. Most theories of ductile fracture address the growth and coalescence process, but the void or crack nucleation and its precursory process seriously affect final fracture.

10.1.1 Void Nucleation

Two models of the dislocation-originated crack formation are shown in Fig. 9.2. Stroh's model assumed pileup at grain boundaries of dislocations moving along a slip band. Difficulties of the model to operate as an incipient crack in hydrogen-induced brittle fracture are stated in Sect. 9.1, but strain incompatibility between the matrix metal and second phase particles is viable to cause separation of the interface. Void nucleation at second phase particles are commonly observed for various metals and alloys as documented in a review article [1]. Cracking and interface decohesion of second phase particles often appear on fracture surfaces.

Some theoretical models have been presented for the cavity formation from second phase particles [2, 3]. The criterion proposed by Argon et al. for the cavity formation is that the interfacial stress reaches the ideal shear strength of the interface provided that sufficient elastic energy available to create new surfaces is stored [2]. The size and distribution of particles are parameters in the criterion originating in interactions of stress fields produced by particles. Argon et al. noted

M. Nagumo, *Fundamentals of Hydrogen Embrittlement*,
DOI 10.1007/978-981-10-0161-1_10

that small cavities less than about 100 nm are difficult to open up spontaneously because the stored elastic energy is insufficient.

The energy criterion for the formation of cavity at a particle by interface separation is given as,

$$\Delta E_{el} + \Delta E_s \leq 0, \tag{10.1}$$

where ΔE_{el} and ΔE_{s} are respectively the internal elastic energy of the particle and the energy increase in forming the new internal surfaces [3]. ΔE_{el} is a function of the stress acting at the particle. Goods and Brown expressed the criterion in terms of the critical strain taking into account the local stress exerted by dislocations near the particle [3]. The critical strain is proportional to the particle size and also depends on the particle shape, coarseness of slip and temperature.

On the other hand, fine dimples not associated with second phase particles are often found, and the refinement of the dimple size characterizes fracture surfaces of hydrogen embrittlement as described in Sect. 7.1(b). Void nucleation without second phase particles was revealed at grain and twin boundaries in titanium alloys [1], at the crack front in AISI 310 stainless steel foils [4] and in high purity single crystal silver foils [5]. Intense strain localization likely characterizes the sites for the void nucleation. A feasible origin of voids is the condensation of vacancies [4]. Generation of vacancies by interactions of moving dislocations is described in Sect. 3.2.1(b), and calculated concentration of vacancies generated by jogged dislocations is shown in Fig. 3.3 [6] as a function of axial plastic strain.

Excess vacancies might diffuse away or annihilate at sinks, but Cuttiño and Ortiz pointed out possible mechanisms to stabilize vacancy aggregates [6]; (1) the reduction in the free energy of the system by condensation of vacancies into clusters or voids, and (2) the reduction in the surface energy by chemisorption of impurity gas such as oxygen. However, the size of voids resulted from vacancy agglomeration is still very small and some mechanisms must operate to induce their growth and/or their link with the main crack.

10.1.2 Void Growth and Coalescence

Cuttiño and Ortiz simulated using a finite element method (FEM) the growth of an initial void by successive diffusing-in of vacancies and its coalescence with the main crack for Cu bicrystal [6]. Assuming the void nucleation by jogged dislocations, the growth of the void radius a during the time interval Δt was expressed as

$$\Delta a = \frac{1}{a} D(c_0 - c_s)\mathrm{d}t, \tag{10.2}$$

where D is the diffusion coefficient of vacancy, c_0 and c_{s} are respectively vacancy concentrations in remote areas and at the boundary of the void. The void grows until

it reaches a critical size and then coalesces with the main crack. When D was assumed to be 10^{-6} m^2/s, the void was predicted to grow from the initial radius of 0.6 nm to the maximum of $230b$ with the vacancy concentration of 6.3×10^{-5}. The assumed magnitude of D was very large as the value at room temperature, and Cuttiño et al. postulated pipe diffusion of vacancies along dislocation lines.

The void growth is strongly affected by stress states. Deformation of fully plastic materials containing sets of cylindrical holes of elliptical cross section was calculated by McClintock in the regime of continuum mechanics [7]. In the model, a hole of semiaxes a and b with a cylindrical axis in the z-direction is surrounded by a cylindrical cell whose dimensions are of the order of the mean spacing between the holes. For plane-strain deformation of a hole in an infinite media, the relative growth factor is defined as

$$F_{zb} = \left(\frac{b}{l_b}\right) \Big/ \left(\frac{b^0}{l_b^0}\right), \tag{10.3}$$

where b, l and the superscript 0 denote radius, spacing and the initial value, respectively. The condition of fracture is that the growth of the holes is such that each hole touches a pair of its cell walls. The relative hole-growth factor at fracture due to z holes growing together in the b direction is

$$F_{zb}^f = \left(\frac{1}{2}\right) \Big/ \left(\frac{b^0}{l_b^0}\right). \tag{10.4}$$

Fracture occurs on the ij-plane when the ij growth factor is the first to reach F_{ij}^f. For tests with a varying stress history, fracture is thought to occur when accumulation of "damage", defined as

$$d\eta_{ij} = d\left(\ln F_{ij}\right)/\ln\ F_{ij}^f, \tag{10.5}$$

reaches unity.

The hole growth with increasing strain was calculated in terms of F_{zb} for viscous and plastic materials under different stress ratios. Stress triaxiality and strain hardening strongly affect fracture strain. Strain hardening is expressed as

$$\overline{\sigma} = \sigma_1 \overline{\varepsilon}^n \tag{10.6}$$

for equivalent stress $\overline{\sigma}$ and strain $\overline{\varepsilon}$. The smaller n enhances the more pronouncedly hole growth. The increase in damage with increasing strain is expressed approximately as

$$\frac{d\eta_{zb}}{d\overline{\varepsilon}} = \frac{\sinh\left[(1-n)(\sigma_a+\sigma_b)/\left(2\overline{\sigma}/\sqrt{3}\right)\right]}{(1-n)\ln F_{zb}^{f}}. \tag{10.7}$$

When ratios between components of applied stress are constant, integration of Eq. (10.7) gives the fracture strain required for z-axis holes to coalesce in the b direction as

$$\overline{\varepsilon}^{f} = \frac{(1-n)\ln\left(l_b^0/2b^0\right)}{\sin\mathrm{h}\left[(1-n)(\sigma_a+\sigma_b)/\left(2\overline{\sigma}/\sqrt{3}\right)\right]}. \tag{10.8}$$

Equations (10.7) and (10.8) indicate strong effects of the transverse principal stress on reducing fracture strain rather than solely the mean stress or the maximum principal stress. The equations also show interaction between stress triaxiality and strain hardening. The effect of triaxiality is the more significant by the smaller hardening exponent.

On tensile straining of materials, necking of specimens is a crucial stage of ductile fracture. Thomason applied the notion to the coalescence of voids within materials [8]. His internal necking model is schematically shown in Fig. 10.1 [8] for initially a square array of small square holes in a plane-strain plastic field. The material is non-hardening rigid-plastic under the hydrostatic pressure P. A tension applied in the X_1 direction causes the deformation of holes. The deformation of the region between adjacent holes is constraint by outside regions of the holes against necking to take place. The constraint changes by straining associated with the change of the geometry of holes. Unstable plastic flow begins when the load L_n to

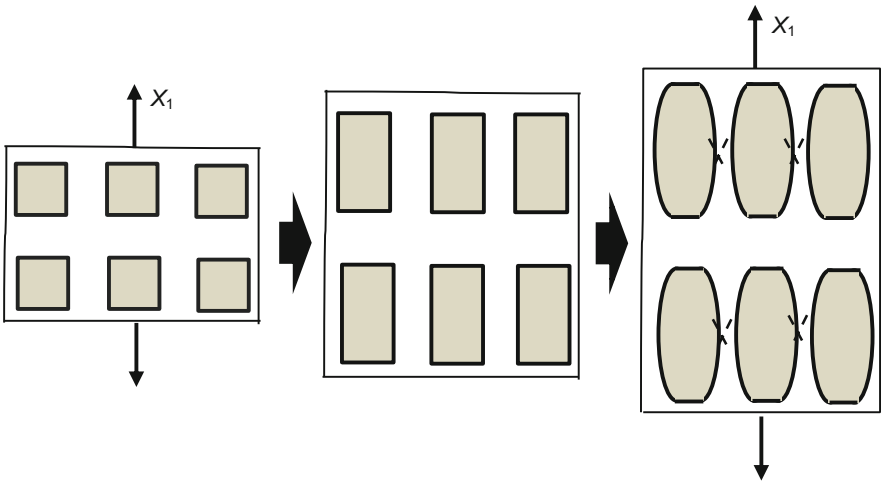

Fig. 10.1 Model of void linking by internal necking. Initially, a square array of small square holes is placed within a matrix (After Thomason [8])

cause internal necking is less than the load L_u for uniform flow. The mean tensile stress σ_n in the X_1 direction to start internal necking was given as,

$$\sigma_n\left(1-\sqrt{V_f}\right)+P<\sigma_{22}+2\tau_y, \tag{10.9}$$

where V_f is the volume fraction of holes, σ_{22} is any tensile stress applied in the X_2 direction and τ_y is the yield shear stress. Effects of V_f, P and σ_{22} on the post-instability strain, *i.e.* the amount of strain from the onset of macroscopic instability to the start of internal necking, were computed. The post-instability strain is significantly reduced by larger V_f and σ_{22} while P suppresses the reduction.

10.1.3 Plastic Instability

Internal necking is a localized breakdown of stability causing strain localization. The treatment of the problem by Thomason regarded the void coalescence as a discontinuous transition in material response from incompressible to dilatational plasticity [9]. Plastic instability that appears in hydrogen embrittlement is described in Sect. 7.2.2 about strain localization. Various factors which influence premature failure associated with plastic instability are reviewed by Onyewuenyi [10]. Plastic instability in homogeneous deformation is characterized by jump discontinuities in displacement gradient across certain surfaces such as shear bands, and it is predicted from continuum mechanics. Plastic instability is induced by materials flow in specific crystallographic planes and directions, microstructural or geometrical inhomogeneities such as inclusions, voids and free surfaces.

Rudnick and Rice assumed that instability is a bifurcation from homogeneous deformation of an initially uniform material to the localization of deformation into a planar band [11]. In an incipient non-uniform field, deformation rates vary with positions across the band but remain uniform outside the band. The coordinate system for the band is shown in Fig. 10.2 [11].

The macroscopic constitutive relation of the material is crucial. The treatment by Rudnick and Rice originally addressed fracture of brittle rock masses. For the material, elastic-plastic constitutive relations were adopted in a pressure and temperature regime showing apparent macroscopic inelastic strain and dilatancy. Shear and volumetric strain increments $d\gamma$ and $d\varepsilon$, respectively, and their plastic portions, $d^p\gamma$ and $d^p\varepsilon$, are written as

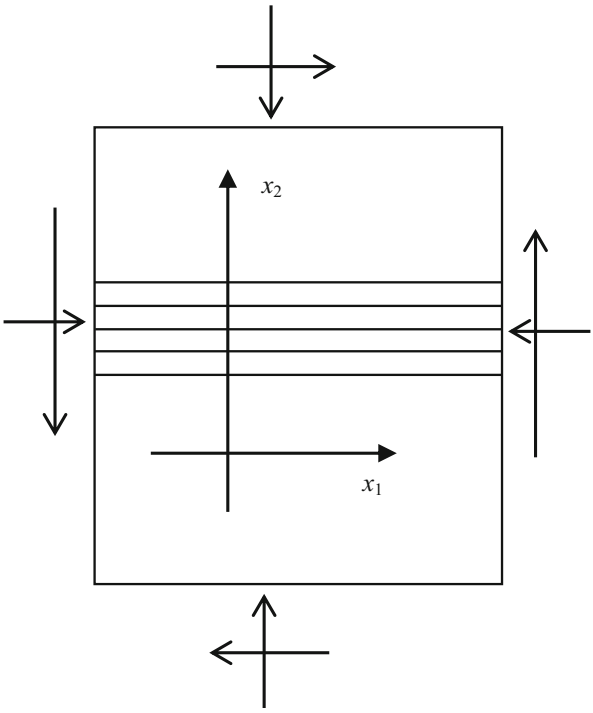

Fig. 10.2 Coordinate system for the band of localization (Rudnicki et al. [11])

$$d\varepsilon = -(d\sigma/K) + d^p\varepsilon, \quad d\gamma = (d\tau/G) + d^p\gamma, \tag{10.10}$$

and

$$d^p\varepsilon = \beta d^p\gamma, \tag{10.11}$$

where σ is the hydrostatic stress, K and G are bulk and shear moduli, respectively, and β is the dilatancy factor. Further, the plastic hardening modulus h is defined as

$$d\tau = hd^p\gamma, \tag{10.12}$$

for constant σ. The shear stress τ *vs.* shear strain γ curve is shown in Fig. 10.3 [11].

The condition for instability was derived from the continuity of stress equilibrium to be satisfied until the start of bifurcation. The hardening modulus h varies by the orientation of the potential plane of localization and plays an important role in the instability condition. The orientation of the plane of localization requires h to be the maximum with respect to the components of the unit normal to the plane in the principal directions. The magnitude of h is a decreasing function of the amount of strain and instability takes place at the critical value h_{cr}. Stress states, values of β, and the slope of the τ *vs.* σ curve are factors that determine h_{cr}. Rudnick and Rice noted that the start of rupture was feasibly modeled as a constitutive instability.

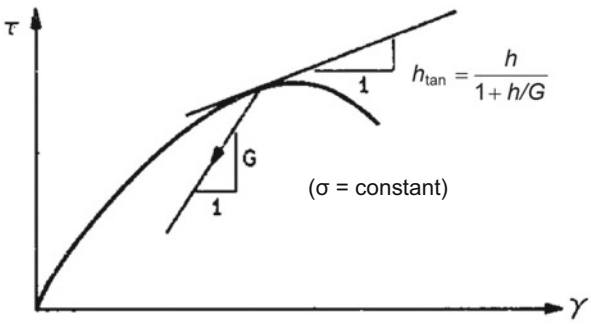

Fig. 10.3 Shear stress τ *vs.* shear strain γ curve showing the geometric interpretation of the hardening modulus h ($= d\tau/d^{p}\gamma$), the tangent modulus h_{tan} and the elastic shear modulus G. $^{p}\gamma$ denotes plastic portion of shear strain Rudnicki et al. [11])

The presence of voids is essential for ductile fracture. A constitutive relation in terms of the yield function Φ for porous material was given by Gurson [12, 13], and a form modified by Tvergaard for the bifurcation instability problem is

$$\Phi = \frac{\sigma_{eqv}^2}{\sigma_y{}^2} + 2f\,q_1 \cos h\left(\frac{3q_2\sigma_m}{2\sigma_y}\right) - \left(1 + q_3 f^2\right) = 0 \tag{10.13}$$

where σ_{eqv} is the equivalent tensile stress, σ_y is the matrix flow stress, σ_m is the macroscopic mean stress, f is the void volume fraction and qs are numerical parameters [14]. $\Phi = 0$ must be satisfied at any stage of the deformation.

Needleman and Tvergaard applied Eq. (10.13) to ductile fracture of materials containing voids adopting $q_1 = q_3 = 1.5$ and $q_2 = 1$ [15]. Equation (10.13) implies that the increase in the void volume fraction lowers flow stress. The void volume fraction f increases during straining by the nucleation of new voids and the growth of existing voids. Then, the increasing rate $\dot{f}$ consists of two terms,

$$\dot{f} = \dot{f}_{\text{nucleation}} + \dot{f}_{\text{growth}}. \tag{10.14}$$

Each term in the right-hand side was given in forms of

$$\dot{f}_{\text{growth}} = (1-f)G^{ij}\,\dot{\eta}_{ij}^{p}, \tag{10.15}$$

and

$$\dot{f}_{\text{nucleation}} = B\left(\dot{\sigma}_y + \dot{\sigma}_m\right) + D\,\dot{\varepsilon}_M^{p}. \tag{10.16}$$

where G^{ij} is the metric tensor that defined the stress deviator $s^{ij} = \sigma^{ij} - G^{ij}\,\sigma_m$, The $\dot{\eta}_{ij}^{p}$ is the plastic part of the macroscopic strain rate and $\dot{\varepsilon}_M^{p}$ is the effective plastic strain rate. For plastic strain-controlled void nucleation, the increasing rate of void volume fraction is written as,

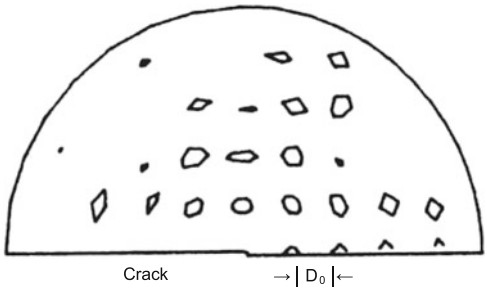

Fig. 10.4 The distribution of large particles near the initial crack tip in model material. Contours depict a constant value (=0.004) of the stress-controlled void nucleation amplitude f_N in Eq. (10.18). D_0 is the initial distance between particles center (Needleman et al. [15])

$$\dot{f}_{\text{nucleation}} = \frac{f_N}{s_N\sqrt{2\pi}} exp\left[-\frac{1}{2}\left(\frac{\varepsilon_M^p - \varepsilon_N}{s_N}\right)^2\right] \dot{\varepsilon}_M^p, \tag{10.17}$$

where f_N is the volume fraction of void nucleating particles, ε_N is the mean strain for nucleation and s_N is the corresponding standard deviation. For stress-controlled void nucleation with the mean stress σ_N for nucleation,

$$\dot{f}_{\text{nucleation}} = \frac{f_N}{s_N\sqrt{2\pi}} exp\left[-\frac{1}{2}\left(\frac{(\sigma_y + \sigma_m) - o_N}{s_N}\right)^2\right] (\dot{\sigma}_y + \dot{\sigma}_m). \tag{10.18}$$

The model material that Needleman and Tvergaard employed contained two types of particles: large particles that nucleate voids at relatively small strains and small particles that nucleate voids at much greater strains. The large particles were placed in regular arrays and the void nucleation was assumed stress-controlled. On the other hand, small particles were uniformly distributed and the void nucleation was strain-controlled. Figure 10.4 [15] shows an example of the model distributions of large particles near the initial crack which is represented by a semi-circular notch. Contours in the figure denote a constant value (=0.004) of the volume fraction of void-nucleating particles and D_0 is the initial distance between particle centers.

Stress and strain fields were computed using a finite element method, and the crack growth in ductile fracture was ascribed to the coalescence of the nearest large void with the crack tip. Ductile fracture is dominated by the interaction between the crack tip and the nearest large void, or between two neighboring large particles. An important implication is that the nucleation of small voids in the ligament between the crack tip and the large void is crucial and that the void volume fraction remains very low in the material near the surface of the growing crack. The criterion for the coalescence is that the void volume fraction in the ligament reaches a critical value, implicitly imaging the loss of the stress-carrying capacity.

The coalescence of the crack tip with a neighboring large void is characterized by the appearance of a small jog in the crack opening displacement *vs* J-integral curves as schematically shown in Fig. 6.11 [15]. The prediction was experimentally

justified for the stable crack growth initiation at three-point bending tests of low carbon steel [16]. Hydrogen effects promoting the onset of the slow crack growth without a large step-wise advance are described in Sect. 6.2.1 with Fig. 6.12. Needleman and Tvergaard assumed homogeneously distributed small particles as the nucleation sites of small void [15]. Uniformly distributed strain-controlled nucleation sites are essential, but their model does not specify the origin of voids and allocates aggregates of vacancies.

10.2 Hydrogen-Enhanced Localized Plasticity Theory

Beachem observed a pronounced decrease in torque by hydrogen for torsion tests of AISI 1020 steel pipe specimens [17] as described in Sect. 5.2(b). Simultaneously conducted wedge-loaded compact tension tests for AISI 4340 steel revealed successive changes in the fracture mode with decreasing stress intensity factor, as described in Sect. 7.1(f). Beachem postulated that hydrogen in solid solution increases dislocation activity and expands a plastic zone ahead of the crack tip containing more inclusions that act as void nuclei. The model is hydrogen-assisted cracking, HAC, rather than the intrinsic embrittlement by hydrogen. However, the effects of hydrogen on the macroscopic flow stress are not yet conclusive and hardening rather than softening has been commonly reported for bulky specimens of commercial grade steels.

Many experiments that exhibit involvement of plasticity in HE, even for apparently brittle-like fracture, are described in Sect. 7.1. Enhanced mobility of dislocations revealed by in situ observations under hydrogen atmosphere, described in Sect. 5.4, is a strong base of notions that claim the primary role of plasticity in HE. The hydrogen enhanced localized plasticity (HELP) has been theoretically rationalized with respect to the shielding of elastic interactions between dislocations and between dislocations and other stress centers as shown by Eq. (5.11) in Sect. 5.5.1. However, numerical estimations showed that fairly high hydrogen concentrations over 0.01 are necessary to exhibit the shielding effects by hydrogen. First-principles calculations have been conducted on interactions between hydrogen and screw dislocations, Sect. 3.1.2, and on the mobility of dislocations, Sect. 5.5.2.

The defect acting agent (DEFACTANT) mechanism described in Sect. 3.1.2 for the stabilization of lattice defects by hydrogen is a general concept from thermodynamic viewpoint. With respect to HELP, the DEFACTANT mechanism predicts that the decrease in the formation energy by hydrogen activates dislocation sources [18]. It was then deduced that newly generated dislocations push former dislocations together with the ease of kink pair formation and that the sequence appears as the observed enhanced mobility of dislocations by hydrogen [19].

The HELP mechanism is viable, but the enhanced dislocation mobility per se is a deformation mechanism, not the mechanism of plastic fracture. As described in Sect. 7.1(d), Martin et al. postulated that the formation of very small ~50 nm mounds immediately beneath the fracture surface of pipe-line steels is a

consequence of either near-surface relaxations of newly created surfaces or reflections of underlying dislocation structures [20]. However, the proposed function of HELP in forming the mounds is no more than to prepare high dislocation densities and hydrogen concentrations [20]. Strain discontinuities brought about at internal boundaries or deformation bands are viable to create voids as Nibur et al. postulated [21], but the conditions for the void nucleation such as Eq. (10.1) must be satisfied. Further, close examinations of similar fracture surfaces revealed nanovoid nucleation and growth [22] rather than "mound-on-valley" separation that Martin et al. claimed. The findings are against the interface separation induced by strain discontinuity as the result of the HELP mechanism.

A notion that relates the HELP mechanism to promoted fracture is a synergistic interplay of the HELP and HEDE mechanisms as proposed by Novak et al. [23] described in Sect. 9.4.1. There, the fracture criterion was essentially that of brittle fracture models. The idea was extended as the HELP-mediated decohesion model to mound-like quasi-cleavage fracture surfaces of pipeline steels [20]. The model postulates that hydrogen transported by activated dislocations causes decohesion at grain boundaries or martensite lath boundaries [24, 25].

On the other hand, a mechanistic consequence of the HELP mechanism to promote fracture was presented by Liang et al. [26] following the theory of plastic instability presented by Rudnicki and Rice [11]. Liang et al. employed a constitutive relation expressing the flow stress σ as a function of the total hydrogen concentration c (in H/M) in the form

$$\sigma(\varepsilon^p, c) = \sigma_0(c)(1 + \varepsilon^p/\varepsilon_0)^N, \tag{10.19}$$

where $\sigma_0(c)$ is the yield stress, ε^{p} is the effective plastic strain, ε_0 is the yield strain and the hardening exponent N was assumed to remain unaltered by hydrogen. The form of $\sigma_0\,(c)$ was tentatively assumed using a softening parameter ξ in the form

$$\sigma_0(c) = \sigma_0\{(\xi - 1)c + 1\}. \tag{10.20}$$

Stress-strain curves in terms of the normalized effective stress $\sigma_{\mathrm{e}}/\sigma_0$ plotted against ε^{p} are shown in Fig. 10.5 [26] taking $\xi = 0.1$, $N = 0.1$, and σ_0 (the yield stress for $c = 0$) $= 400$ MPa.

Hydrogen-induced lattice dilatation due to the partial molar volume of hydrogen was included in the deformation rate tensor. An important assumption was that hydrogen is supplied from environment during the test keeping the chemical potential of lattice hydrogen constant at c_0. It was assumed that the total hydrogen concentration c increases due to trapping by the increasing density of dislocations during straining. The assumptions imply that hydrogen trapped in dislocations decreases the flow stress and enhances the decrease in strain hardening.

The employed condition of plastic instability is the model by Rudnicki-Rice for the bifurcation from continued homogeneous deformation to a localized deformation in a band of intense shear. The results of calculations following Rudnicki-Rice's procedure are shown in Fig. 10.6 [26] in terms of the hardening modulus

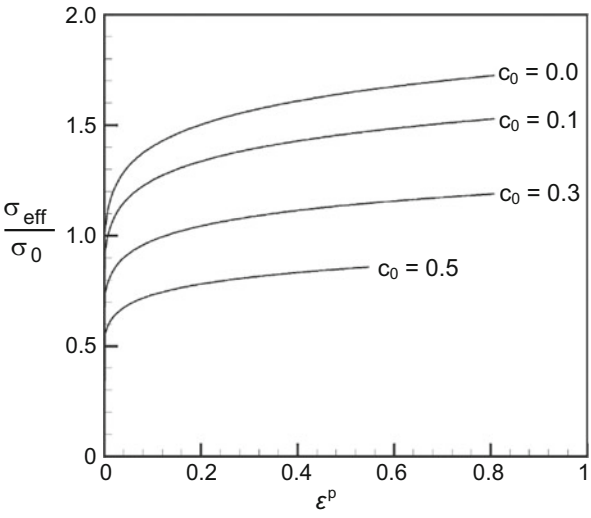

Fig. 10.5 Normalized effective stress σ_{eff} *vs.* plastic strain ε^{p} curves at various initial hydrogen concentrations c_0 calculated using Eqs. (10.19) and (10.20). The hardening exponent $N = 0.1$, the softening parameter $\xi = 0.1$ and σ_0 is the yield stress in the absence of hydrogen (Liang et al. [26])

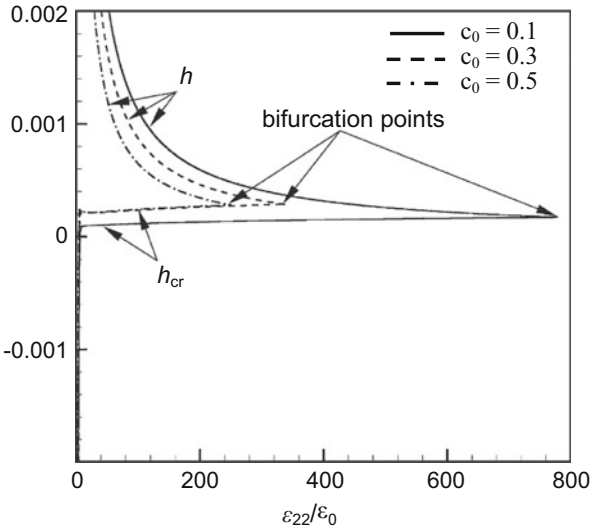

Fig. 10.6 Plot of the tangential modulus h and the critical tangent modulus h_{cr} against the normalized applied macroscopic strain $\varepsilon_{22}/\varepsilon_{\text{o}}$ at various initial hydrogen concentrations. The hardening exponent $N = 0.1$ and the softening parameter $\xi = 0.1$, and shear localization occurs when $h = h_{\text{cr}}$ (Liang et al. [26])

h against the normalized applied macroscopic strain for three initial hydrogen concentrations. The modulus h is defined as

$$h = \left[\frac{\partial \sigma_e}{\partial \varepsilon^p} + \left(\frac{\partial \sigma_e}{\partial c}\right)\left(\frac{\partial c}{\partial \varepsilon^p}\right)\right] \Big/ 3. \tag{10.21}$$

External tensile stress is applied along the x_2 direction, and the bifurcation takes place when h that decreases with increasing ε_{22} reaches the critical value h_{cr}. The

higher initial hydrogen concentrations decrease h the more promptly and reduce the critical strain for the bifurcation the more prominently.

Hydrogen-induced softening and lattice dilatation at micro-scale regions can induce shear localization even though the material as a whole continues to exhibit positive hardening. The idea might be qualitatively reasonable, but Fig. 10.6 indicates that unrealistically high initial hydrogen concentrations, ≥ 0.2 in atomic ratio, are required to cause discernible reductions in the uniform elongation. The misfit with experimental observations might be improved by modified flow rules, but consistency with characteristic features of hydrogen embrittlement, such as fracture surfaces described in Sect. 7.1, is a subject to be further examined.

10.3 Adsorption-Induced Dislocation Emission Theory

Fractographic features such as fine, shallow dimples, striations, quasi-cleavage with steps and tear ridges that characterize hydrogen embrittlement (Sect. 7.1) are quite similar to the features of stress corrosion cracking (SCC) and liquid-metal embrittlement (LME). Since LME occurs even at high crack velocities and for systems of very low mutual solubilities, Lynch proposed that some surface effects such as the adsorption of hydrogen at crack tips play a critical role in hydrogen embrittlement [27, 28]. For LME, adsorption must occur only at crack tips and Lynch proposed a model that adsorbed hydrogen enhances the injection of dislocations from the crack tip and promotes the coalescence of the crack with voids ahead of the crack.

The elementary fracture mode envisaged is the microvoid coalescence (MVC) process. The qualitative explanation is that adsorbed hydrogen at crack-tip reduces the interatomic strength of metals and facilitates the dislocation nucleation and injection into the bulk. This adsorption-induced dislocation emission (AIDE) mechanism also claims that hydrogen at subsurface sites is able to contribute to bond-weakening. Void nucleation at small and large particles was assumed in areas of large strain such as localized slip around crack tips, slip band intersections or dislocation-cell boundaries.

Both the HELP and AIDE mechanisms consider the function of hydrogen in fracture from the viewpoint of strain localization for inducing void nucleation. The difference between the two mechanisms is that HELP focuses on the dislocation mobility enhanced by hydrogen while AIDE considers the enhancement of the dislocation injection from the surface. The mechanism addressed to transgranular fracture was also applied to apparently smooth intercrystalline facets that exhibited small dimples. Lynch assumed second phase particles as the void source, but he noticed the existence of dimples not associated with particles, smaller than dimples produced in air, sometimes difficult to resolve by scanning electron microscopy. The origin of such mall voids was not inquired. The AIDE model addresses fractographic features that associate with the crack extension. However, similar

fractographic features appear for embrittlement caused by internal hydrogen which also promotes accumulation of damage as described in Sect. 7.3 characterizing hydrogen embrittlement.

10.4 Autocatalytic Void-Formation and Shear-Localization Theory

Flow localization into shear band induced by plastic instability is a critical stage in ductile fracture as described in Sect. 10.1.3. In terms of continuum mechanics, a low macroscopic strain-hardening rate favors instability. However, very large strain and hydrogen concentrations are necessary to initiate flow bifurcation in a homogeneous material according to a computation based on the HELP mechanism as shown in Fig. 10.6. On the other hand, microstructural or geometrical inhomogeneities also cause flow localization. Hydrogen effects on enhancing strain localization along characteristic slip lines at the U-notch root of a bend specimen of spheroidized steel are shown in Fig. 7.15 in Sect. 7.2.2. Reentrant portions of a roughened surface as well as particles within slip bands act as trigger sites of plastic instability, but the onset of surface rumpling occurred well before the profuse void formation was attained in the bulk [29]. Associated degradation in fracture toughness is shown in Fig. 6.10 in Sect. 6.2.1 about mixed mode I/III compact tension tests. It was then deduced that the major role of hydrogen is to promote plastic instability directly [29].

Hirth et al. proposed the autocatalytic model of hydrogen embrittlement, claiming that the nucleation of voids enhances the formation and propagation of shear bands in which voids are further formed [30, 31]. The function of hydrogen was ascribed to promote particle decohesion or cracking at second phase particles. The model does not require the HELP mechanism for the dislocations activity but implicitly assumes high hydrogen fugacity for the interface decohesion. As stated in Sect. 7.2.2, the steels used for experiments had a substantial ductility before fracture. A similar U-notch bend test was conducted for a high strength AISI 4340 steel of 1.35 GPa in tensile strength. The midspan-deflection at the onset of load drop was progressively reduced with the increasing current density of cathodic electrolysis [32]. In the midplane section of precharged specimens, a narrow mode II crack extended following characteristic slip paths and the length of the spiral part of the crack increased with decreasing charging current. The extending crack connected to mode I intergranular cracks in a region apart from the notch surface. In contrast to low strength steels, it was considered that the crack initiated internally first and connected to the surface. However, the critical notch-root strain at the crack initiation was nearly constant for three different notch-root radii.

It was deduced that the dominant role of hydrogen is to promote plastic instability and that the crack nucleation within the plastic zone is the consequence of a combination of the hydrogen concentration and the total stress. On the fracture surface, MnS was observed at the bottom of large dimples, but the origin of small dimples that became smaller and more uniform by hydrogen charging was not definitely mentioned. Experiments that the theory based on were mostly conducted under a high hydrogen fugacity, but the underlying idea of the auto-catalytic model about plastic instability will be generally provided that the void source is not limited to second phase particles as will be stated in the following section.

10.5 Hydrogen-Enhanced Strain-Induced Vacancy Theory

Plastic deformation is deeply involved in hydrogen embrittlement (HE), and the primary player of plasticity is the dynamics of dislocations. Functions of dislocations in fracture are multiple. The increase in the density of dislocations and their interactions set up substructures and local stress and strain fields in which fracture events take place. On the one hand, dislocation dynamics also bring about damage that deteriorates mechanical performance of materials. The term "damage" here denotes in a broader sense deterioration of crystallinity rather than flaws such as cracks and voids. The function of hydrogen in embrittlement is to be considered in the context of dislocation dynamics and resultant microstructural changes.

The hydrogen-enhanced strain-induced vacancy (HESIV) mechanism proposed by Nagumo [33] claims that hydrogen enhances the strain-induced creation of vacancies leading to premature fracture. Excess vacancies are stabilized and their mobility is reduced by combining with hydrogen, thus forming clusters that act as void sources or reducing the stress-carrying capacity of the material. Figure 10.7 illustrates the creation and clustering of vacancies forming microcracks in strain-concentrated area close to a barrier for the slip extension. The HESIV mechanism has shifted the viewpoint on HE from hydrogen itself to hydrogen-related damage that leads to premature fracture.

Fig. 10.7 Illustration of the HESIV model for the creation and clustering of vacancies forming microcracks in strain-concentrated area close to a barrier for slip extension

10.5.1 Brief Summary of Findings

(a) Hydrogen-enhanced creation of strain-induced vacancies

The creation of vacancies associated with plastic straining has been exhibited by means of thermal desorption analysis of hydrogen as shown in Fig. 3.2 for iron and in Fig. 2.4 for eutectoid steel. Hydrogen was introduced as the tracer of lattice defects, and the increase is fairly general for other steels and alloys. The vacancy-type nature of the lattice defects trapping hydrogen was demonstrated by annealing experiments of strained materials by means of thermal desorption analysis (TDA) as shown in Fig. 3.2 and in Figs. 3.8, 3.9 and 3.10. The vacancy-type nature of strain-induced defects is confirmed by positron annihilation spectroscopy (PAS) which is a more direct method to identify vacancies and their clusters. The PAS results shown in Figs. 3.11 and 3.12 are consistent with TDA results. The crucial finding is that hydrogen enhances preferentially the creation of vacancies as shown in Table 3.4.

Ion-implantation experiments shown in Fig. 3.6 and Table 3.3 validate high densities of vacancies due to the stabilization by hydrogen. Ion-implantation experiments also revealed the decrease in the mobility of vacancies by coupling with hydrogen and by forming clusters. Theoretical estimations of high densities of vacancies resulting from interactions between dislocations are described in Sect. 3.2.1(b). Binding of hydrogen with vacancies reduces the formation energy and then increases the density of vacancies as described in Sect. 3.2.3(b). Further, a first-principles calculation on the mobility of vacancies predicted a high density of vacancies left behind jog-dragging of screw dislocations as the result of coupling with hydrogen. The findings support the notion that interactions between hydrogen and excess vacancies result in high densities of vacancies and their clusters.

(b) Correlations with the susceptibility to hydrogen embrittlement

Compositions and microstructures strongly affect the susceptibility to hydrogen embrittlement of steels even of the same strength levels. The origins are ascribed to the extent of the strain-induced creation of vacancies. Good correlations between the susceptibility and the amount of strain-induced vacancies are demonstrated for high strength martensitic steels with the prior austenite grain size effects in Figs. 8.6 and 8.7 and manganese content effects in Figs. 7.8 and 8.8. Positron annihilation spectroscopy revealed more prominent clustering of vacancies in Type 304 austenitic stainless steel than in Type 316 L as described in Sect. 7.2.1(b) corresponding to their different susceptibilities to HE.

Strain-rate and temperature dependences of the susceptibility to HE, shown in Fig. 6.3, characterize HE of steels. In tensile tests of cold-worked eutectoid steel, it was demonstrated that the enhanced degradation by reducing the strain rate was associated with increasing amounts of strain-induced vacancies, as shown in Fig. 6.4. In experiments to investigate cumulative effects of loading-modes, cyclic prestressing in the presence of hydrogen degraded tensile properties of martensitic steel. The degradation was more prominent with lower strain rate at cyclic

prestressing as shown in Fig. 7.18, and the effects of strain rates at cyclic prestressing were well related to the absorption capacity of tracer-hydrogen trapped in vacancies, *i.e*. the density of strain-induced vacancies as shown in Fig. 7.19.

(c) Damage accumulation and superposing effects of loading-modes

Deterioration of materials under external stress precedes fracture to take place. Hydrogen-enhanced strain localization and deterioration of crystallinity along twin boundaries are shown in Figs. 7.13 and 7.16, respectively, for Type 304 austenitic stainless steel. Creation of vacancies in the incubation period prior to the onset of fracture was revealed as damage in materials. In sustained-loading delayed fracture tests of high strength steels, the increase in absorbed hydrogen is not monotonic as shown in Figs. 6.23 and 6.24. Time-dependent change of the amount of lattice defects during the incubation period was detected by means of TDA of hydrogen used as the tracer. As shown in Fig. 6.25, the amount of tracer-hydrogen gradually increased with loading-time after an initial drop and its final amount was very high in portions close to the fracture surface. Simultaneously conducted positron annihilation spectroscopy revealed the vacancy-type nature of the defects. Hydrogen enhancement of the creation of defects was revealed in the incubation period of fatigue failure by means of TDA as shown Fig. 6.17 for rotational bending fatigue tests of high strength Si-Cr steel. The results are consistent with the promotion of fatigue failure in the presence of hydrogen.

Hydrogen degradation appears in mechanical tests with various loading-modes, but deterioration of materials preceding the onset of fracture will be common for various tests. Then, hydrogen effects on degradation are cumulative for a material subjected to various loading histories as described in Sect. 7.3.2. Fig. 7.20 for delayed fracture tests of prefatigued Si-Cr martensitic steels demonstrates that damage accumulated during prefatigue promotes fracture in delayed fracture tests. Annealing experiments shown in the figure indicate that damage concerned is vacancies. Figure 7.21 for tensile tests of high strength steel initially subjected to sustained-loading in a corrosive solution shows degradation of tensile properties due to vacancy-type defects introduced by the preceding sustained-loading. Further, the effects of cyclic stressing prior to tensile tests, shown in Figs. 7.18 and 7.19, show the essential role of strain-induced vacancies in degradation through accumulation of damage.

(d) Model experiments for the role of vacancies

Most studies so far conducted for the mechanism of HE remark hydrogen effects on the crack initiation and growth. The HESIV mechanism addresses deterioration of materials rather than hydrogen itself as the essential factor of degradation. A more direct demonstration of the essential role of vacancies in HE was the intermediate unloading and annealing experiments conducted during tensile tests of hydrogenated iron and Inconel 625, shown in Fig. 6.6. It demonstrates that the degradation at tensile tests was caused by vacancy-originated damage produced in the sustained-loading stage while hydrogen was absent at the time of fracture.

10.5.2 Crack Growth Resistance and its Microscopic Origin

The functions of vacancies in the susceptibility to HE must be incorporated in the mechanics of fracture. The crack propagation in ductile fracture proceeds sequentially following the nucleation, growth and linkage of voids. The crack growth resistance curve, *R*-curve, described in Sects. 6.2.1 and 6.2.2(c), gives a link between the total energy dissipation rate and microscopic processes of fracture through the constitutive relation in calculating the *J*-integral.

Figure 10.8 [34] shows *R*-curves obtained by three-point bend tests of three low carbon ferrite-pearlite steels of about 450 MPa in tensile strength. The three steels contain 2 mass % of (Mn + Ni) with varied Mn/Ni ratios, and the compositions resulted in different amounts of carbides along grain boundaries. The steels used for Figs. 6.14 and 7.5 are Steel B and Steel A, respectively, used for Fig. 10.8. The constraint factor, η, is defined as the fraction of grain boundaries length occupied by hard phases, such as carbides and pearlite that block slip extension across grain boundaries, to the total grain boundary length. The values of η are 58.1, 33.2 and 43.5 % for steel A, B and C, respectively.

Lattice defects induced by plastic straining were detected using hydrogen as the tracer. Figure 10.9 [34] shows thermal desorption curves of tracer-hydrogen (tritium in this case) introduced to the three steels strained to 20 % at room temperature. When straining was not given, hydrogen (tritium) absorption capacities were almost the same in the three steels. For strained steels, the amounts of tracer-tritium were the larger for steels with the higher constraint factors, and the tracer-tritium was diffusive at room temperature.

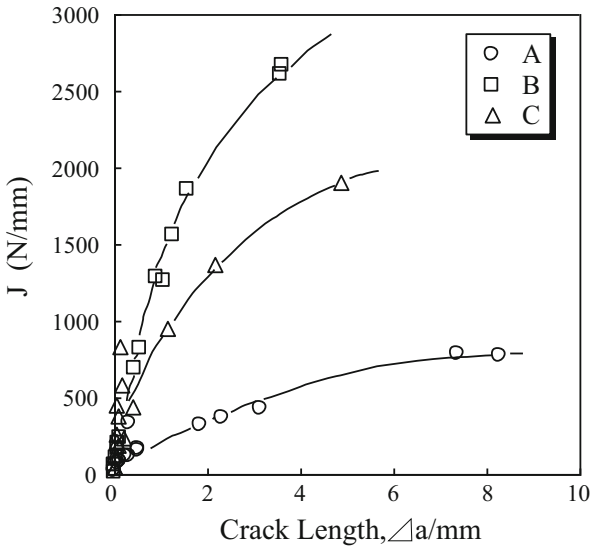

Fig. 10.8 *R*-curves of three low carbon steels of similar compositions except Mn/Ni ratios.for 2 mass % of (Mn + Ni). Three steels have different constraint factors for slip extension across grain boundaries. Tests are conducted at 20 °C (Nagumo et al. [34])

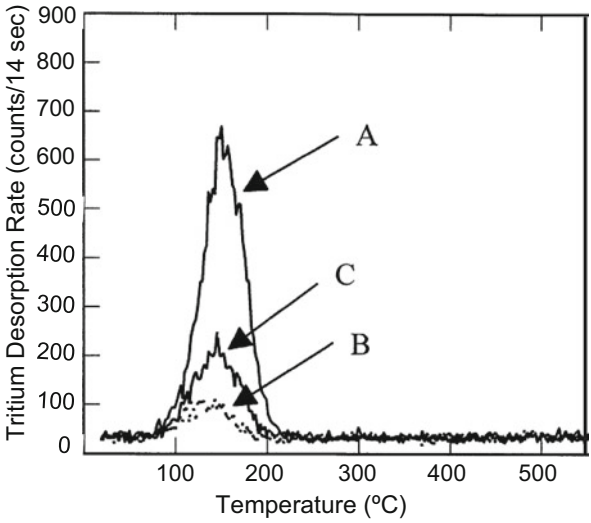

Fig. 10.9 Thermal desorption profiles of tritium introduced to the three steels used in Fig. 10.7 strained to 20 % at 20 °C (Nagumo et al. [34])

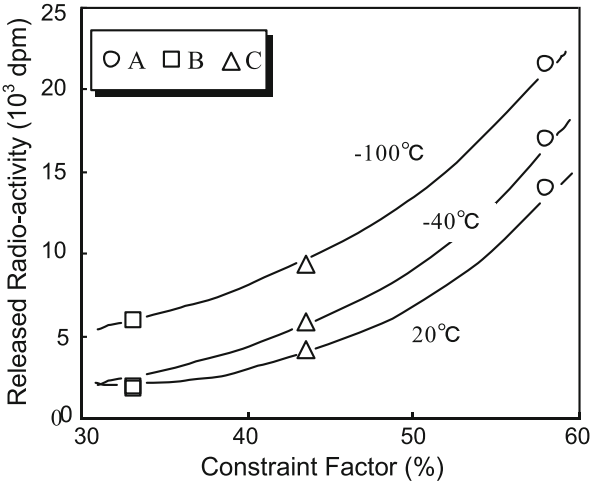

Fig. 10.10 Correlation between the constraint factor and the total amount of the thermally desorbed tritium from the three steels in Fig. 10.7 strained to 20 % at different temperatures (Nagumo et al. [34])

A critical issue is the function of the constraint phases on R-curves. The three steels are characterized by different constraint factors, and Fig. 10.10 [34] plots the amounts of tracer-hydrogen in terms of the released radio-activity (the disintegration per minute, dpm) as a function of the constraint factor for specimens strained to 20 % at different temperatures. The amounts of tracer-hydrogen correspond to those of strain-induced defects. The results imply that the constraint of slip extension, likely due to grain-boundary carbides, causes strain concentration and enhances the creation of strain-induced vacancies that trap tracer-hydrogen. A high density of vacancies leads to the formation of voids and promotes fracture to proceeds. The results correspond to the dependence of *R*-curves on slip constraint shown in Fig. 10.8.

10.5.3 *Simulation of* R-*Curve and Strain Localization Near the Crack-Tip*

The correspondence between R-curves and the density of strain-induced vacancies relates macroscopic mechanics to microscopic processes of fracture. The J-integral is calculated from the stress and strain fields near the crack tip as described in Sect. 6.2.1. Yoshida computed the stress and strain fields near the crack tip by means of a finite element method using the constitutive relations Eq. (10.13) for porous materials and experimentally obtained flow stress [35]. Equation (10.17) was adopted for the calculation of the plastic strain-rate controlled void-nucleation rate using experimentally determined volume fractions of void nucleating particle, f_N. Actually, f_N was measured by a scanning electron microscope on a vertical cross section of specimens subjected to tensile straining up to ε_N just before the maximum stress. The experimental value of f_N for Steel B was 0.02. Void nucleating particles were hard phases such as cementite layer or pearlite existing along grain boundaries.

The J-integral values were calculated at successive extensions of a crack and Fig. 10.11 [35] plots calculated J-integral values on the experimental R-curves for Steel B in Fig. 10.8 at two test temperatures. The agreement between the calculation and experiment is satisfactory. Insensitivity to test temperature is a characteristic feature of R-curve. The simulation of R-curve shown in Fig. 10.11 validated the feature. The origin is the opposite temperature dependencies of the flow stress and strain by canceling each effect on the buildup of strain energy for J-integral [35].

Hydrogen effects on the R-curve shown in Fig. 6.14 are observed with a steel of quite similar compositions as Steel B in Fig. 10.8. Both experimental and computed

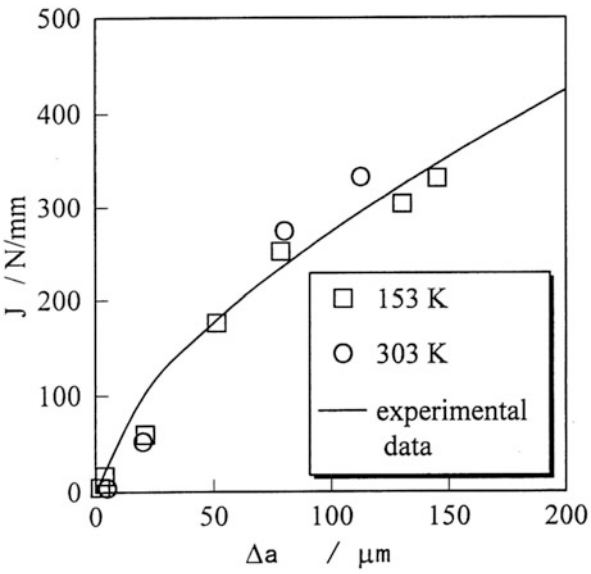

Fig. 10.11 Comparison between calculated and experimental R-curves for Steel B in Fig. 10.7 tested at different temperatures (Yoshida et al. [35])

J-integral values are plotted and the computation was conducted in a similar way as for Fig. 10.11 using values of f_N raised from 0.02 for the hydrogen-free to 0.035 for the hydrogen-charged specimens [36]. It is to be noticed that the constraint phases in the original microstructure were not affected by hydrogen-charging when straining was not applied. The increase in f_N takes place at the time of straining in the presence of hydrogen, and the coincidence of experimental and computational results in Fig. 6.14 represent the mechanistic effect of the HESIV mechanism on the crack growth.

The constitutive relation Eq. 10.13 was also successfully applied to the analysis of the start of stable crack from the pre-crack as described in Sect. 6.2.1. The steel used for Fig. 6.12 is Steel A in Fig. 10.8. The notion common to the crack initiation and propagation is that the increased density of small voids reduces the stress-carrying capacity of the matrix in front of the crack and promotes the onset of plastic instability.

Strain localization is a feature that characterizes deformation at hydrogen embrittlement as described in Sect. 7.2.1, and the intense creation of vacancies is closely related to strain localization. The FEM calculation using the constitutive relation Eq. 10.13 revealed a substantial enhancement of strain localization near the crack-tip when hydrogen was present [36]. Distributions of voids ahead of the crack after the advance of 200 μm were computed for Steel B [36]. Figure 10.12 [36] shows the distribution of the volume fraction of nucleation voids $f_{\text{nucleation}}$ with and without hydrogen charging. The enhanced localization of voids well explains fractographic features of HE such as the refinement of dimple size and quasi-cleavage fracture surface. However, simulations of R-curves shown in Figs. 10.11 and 6.14 are for low carbon ferrite-pearlite steel of a medium strength level. Further examinations for high strength steels are necessary.

10.6 Summary of Ductile Fracture Models

Features characterizing hydrogen embrittlement of steels indicate involvement of plasticity in most cases even for IG fracture of high strength steels. The function of hydrogen on the role of dislocations has been ascribed to either the increase in either the mobility (HELP) or the density (AIDE and DEFACTANT) of dislocations. The mechanistic outcome of activated dislocations, however, is not straightforward to fracture events. Postulated mechanisms are the decrease in the flow stress promoting plastic instability or the increase in the number of piled-up dislocations resulting in the interface decohesion at second phase particles. Alternatively, the HELP-mediated decohesion model postulates enhanced hydrogen transport by activated dislocations to cause decohesion at grain boundaries or martensite lath boundaries. The autocatalytic model remarks synergistic effects of particle cracking by hydrogen and plastic instability induced by the cracks, resulting in the void sheet formation along slip lines. The viability of a model

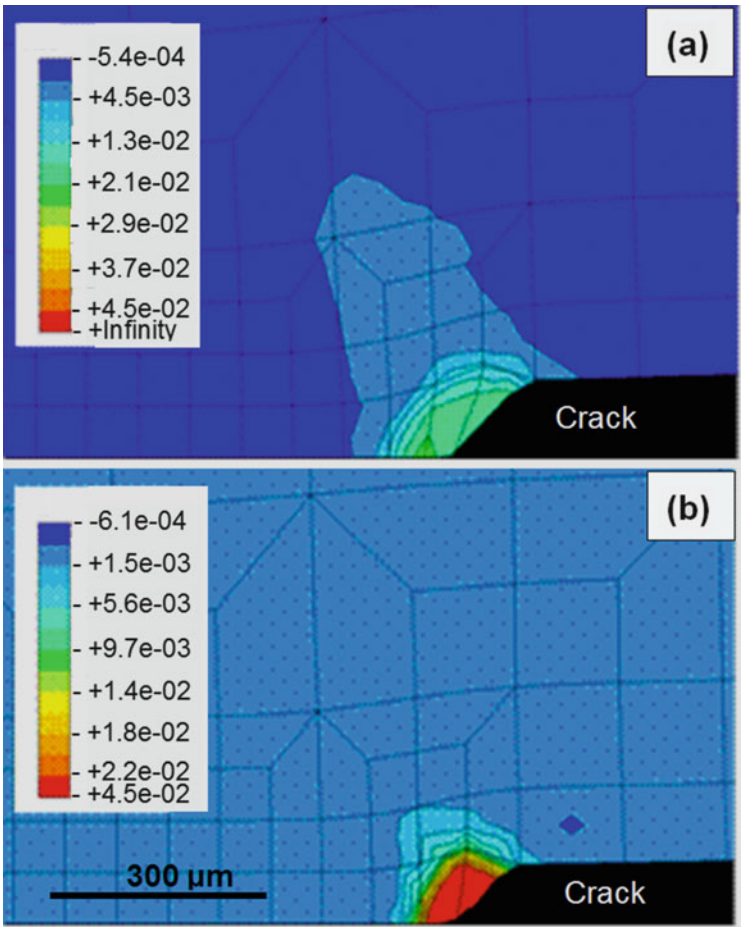

Fig. 10.12 Calculated distributions of nucleation void volume fractions ahead of the crack in Steel B in Fig. 10.7 after the crack advance of 200 μm (**a**) without and (**b**) with hydrogen (Nagumo et al. [36])

should depend on situations where the concentration and the fugacity of hydrogen satisfy fracture criteria.

The HESIV model, on the other hand, remarks on the role of vacancies and their clusters created by interactions between moving dislocations. Hydrogen effects are ascribed to the stabilization of vacancies increasing the density of vacancies and promoting their clustering. The model addresses hydrogen effects in successive stages of fracture; accumulation of damage, initiation of microvoids or cracks and their growth. The constitutive relation that incorporates the void volume fraction that increases with strain for porous materials well describes observed mechanistic behaviors. Clustering of vacancies is postulated as the embryo of voids, but the promoted plastic instability is essential for premature fracture. The function of high

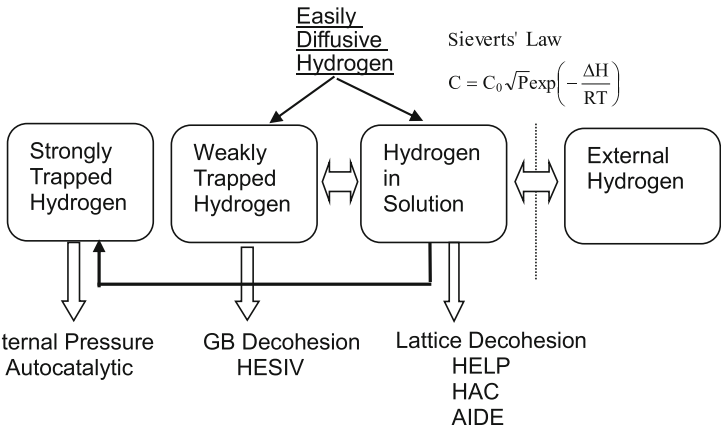

Fig. 10.13 Positions of proposed models for hydrogen embrittlement with respect to states of hydrogen in materials (Nagumo [33])

densities of vacancies on instability caused by deteriorated crystallinity is expected to be described by some other mechanistic treatments.

Major models so far presented on the mechanism of HE are positioned in Fig. 10.13 [33] with respect to the states of hydrogen concerned with each model. Both the HELP and HESIV models premise the role of activated dislocations, but the HESIV claims the primary role of vacancies created by interactions between moving dislocatons. Deformation microstructures that characterize HE such as fractographic features and localized deformation are difficult to discriminate between the two models. For a definite understanding, revealing the entity of nanoscale damage in the entire fracture process would be decisive.

References

1. R.H. Van Stone, T.B. Cox, J.R. Row Jr., J.A. Psioda, Int. Metals Rev. **30**, 157–179 (1985)
2. A.S. Argon, J. Im, R. Safoglu, Metall. Trans. A **6A**, 825–837 (1975)
3. S.H. Goods, L.M. Brown, Acta Metall. **27**, 1–15 (1979)
4. Q.-Z. Chen, W.-Y. Chu, Y.-B. Wang, C.-M. Hsiao, Acta Mater. **43**, 4371–4376 (1995)
5. R.L. Lyles Jr., H.G.F. Wilsdorf, Acta Metall. **23**, 269–277 (1975)
6. A.M. Cuttiño, M. Ortiz, Acta Mater. **44**, 427–436 (1996)
7. F.A. McClintock, Trans. ASME, J. Appl. Mech. **35**, 363–371 (1968)
8. P.F. Thomason, J. Inst. Met. **96**, 360–365 (1968)
9. P.F. Thomason, Acta Metall. **29**, 763–777 (1981)
10. O.A. Onyewuenyi, in *Hydrogen Degradation of Ferrous Alloys*, ed. by R.A. Oriani, J.P. Hirth, M. Smialowski (Noyes Pub, Park Ridge, 1985), pp. 414–453
11. J.W. Rudnicki, J.R. Rice, J. Mech. Phys. Solids **23**, 371–394 (1975)
12. A.L. Gurson, Trans. ASME, J. Eng. Mater. Tech. **99**, 2–15 (1977)
13. A.L. Gurson, in *Fracture 1977, Proc. The 4th Int. Conf. Fracture*, ed. by D.M.R. Taplin, vol. 2 (University Waterloo Press, Wateloo, 1977), pp. 357–364
14. V. Tvergaard, J. Mech. Phys. Solids **30**, 399–425 (1982)

15. A. Needleman, V. Tvergaard, J. Mech. Phys. Solids **35**, 151–183 (1987)
16. Y. Fujii, A. Kikuchi, M. Nagumo, Metall. Mater. Trans. A **27A**, 469–471 (1996)
17. C.D. Beachem, Metall. Trans. **3**, 437–451 (1972)
18. R. Kirchheim, Scr. Mater. **62**, 67–70 (2010)
19. R. Kirchheim, Acta Mater. **55**, 5139–5148 (2007)
20. M.L. Martin, I.M. Robertson, P. Sofronis, Acta Mater. **59**, 3680–3687 (2011)
21. K.A. Nibur, B.P. Somerday, D.K. Balch, C. San Marchi, Acta Mater. **57**, 3795–3809 (2009)
22. T. Neeraji, R. Srinivasan, J. Li, Acta Mater. **60**, 5160–5171 (2012)
23. P. Novak, R. Yuan, B.P. Somerday, P. Sofronis, R.O. Ritchie, J. Mech. Phys. Solids **58**, 206–226 (2010)
24. A. Nagao, C.D. Smith, M. Dadfarnia, P. Sofronis, I.M. Robertson, Acta Mater. **60**, 5182–5189 (2012)
25. M.L. Martin, B.P. Somerday, R.O. Ritchie, P. Sofronis, I.M. Robertson, Acta Mater. **60**, 2739–2745 (2012)
26. Y. Liang, P. Sofronis, N. Aravas, Acta Mater. **51**, 2717–2730 (2003)
27. S.P. Lynch, Acta Metall. **32**, 79–90 (1984)
28. S.P. Lynch, Acta Metall. **36**, 2639–2661 (1988) (overview)
29. O.A. Onyewuenyi, J.P. Hirth, Metall. Trans. A **14A**, 259–269 (1983)
30. J.A. Gordon, J.P. Hirth, A.M. Kumar, N.E. Jr. Moody, Metall. Trans. A **23A**, 1013–1020 (1992)
31. J.P. Hirth, in *Hydrogen Effects on Materials*, ed. by A.W. Thompson, M.R. Moody (TMS, Warrendale, 1996), pp. 507–522
32. T.D. Lee, T. Goldenberg, J.P. Hirth, Metall. Trans. A **10A**, 439–448 (1979)
33. M. Nagumo, Mater. Sci. Tech. **20**, 940–950 (2004)
34. M. Nagumo, T. Yagi, H. Saitoh, Acta Mater. **48**, 943–951 (2000)
35. H. Yoshida, M. Nagumo, ISIJ Int. **38**, 196–202 (1998)
36. M. Nagumo, H. Yoshida, Y. Shimomura, T. Kadokura, Mater. Trans. **42**, 132–137 (2001)